The Journal of Chemical Physics

RESEARCH ARTICLE | SEPTEMBER 20 2023

Relativistic resolution-of-the-identity with Cholesky integral decomposition

Samragni Banerjee ; Tianyuan Zhang ; Kenneth G. Dyall ; Xiaosong Li

J. Chem. Phys. 159, 114119 (2023)
https://doi.org/10.1063/5.0161871

AIP Publishing

The Journal of Chemical Physics ARTICLE pubs.aip.org/aip/jcp

Relativistic resolution-of-the-identity with Cholesky integral decomposition

Cite as: J. Chem. Phys. 159, 114119 (2023); doi: 10.1063/5.0161871
Submitted: 12 June 2023 • Accepted: 28 August 2023 •
Published Online: 20 September 2023

Samragni Banerjee,[1] Tianyuan Zhang,[1] Kenneth G. Dyall,[2] and Xiaosong Li[1,a)]

AFFILIATIONS

[1] Department of Chemistry, University of Washington, Seattle, Washington 98195, USA
[2] Dirac Solutions, Portland, Oregon 97229, USA

[a)] **Author to whom correspondence should be addressed:** xsli@uw.edu

ABSTRACT

In this study, we present an efficient integral decomposition approach called the restricted-kinetic-balance resolution-of-the-identity (RKB-RI) algorithm, which utilizes a tunable RI method based on the Cholesky integral decomposition for in-core relativistic quantum chemistry calculations. The RKB-RI algorithm incorporates the restricted-kinetic-balance condition and offers a versatile framework for accurate computations. Notably, the Cholesky integral decomposition is employed not only to approximate symmetric large-component electron repulsion integrals but also those involving small-component basis functions. In addition to comprehensive error analysis, we investigate crucial conditions, such as the kinetic balance condition and variational stability, which underlie the applicability of Dirac relativistic electronic structure theory. We compare the computational cost of the RKB-RI approach with the full in-core method to assess its efficiency. To evaluate the accuracy and reliability of the RKB-RI method proposed in this work, we employ actinyl oxides as benchmark systems, leveraging their properties for validation purposes. This investigation provides valuable insights into the capabilities and performance of the RKB-RI algorithm and establishes its potential as a powerful tool in the field of relativistic quantum chemistry.

I. INTRODUCTION

In quantum chemistry calculations utilizing the in-core algorithm with an atomic orbital (AO) basis, the memory storage requirement for four-index two-electron repulsion integrals (ERIs) scales as N^4, where N represents the number of basis functions. To address the challenge posed by the rapid scaling of memory requirements, a commonly employed approach in electronic structure calculations is the utilization of the resolution-of-the-identity (RI) formalism, which approximates the 4-index ERI tensor as a product of two 3-index tensors.[1–11] Several approaches have been developed to construct the three-index RI tensors, with the Cholesky decomposition[12–21] and density fitting[22–24] techniques being the most popular.

The density fitting approach, although relatively straightforward to implement, relies on pre-optimized atom-centered auxiliary basis sets. Unfortunately, this method often introduces uncontrolled errors that scale with the size of the system. On the other hand, the Cholesky decomposition technique offers a more robust alternative to density fitting. It constructs the auxiliary basis on-the-fly, eliminating the dependence on standard fitting basis sets. Moreover, the accuracy of the Cholesky decomposition can be adjusted based on a user-defined threshold for any atom-centered basis set. However, the Cholesky decomposition method is more intricate to develop and requires extensive optimization to achieve optimal performance.[19]

Since the initial implementation of the Cholesky decomposition formalism by Beebe and Linderberg,[12] numerous schemes have been proposed to enhance its efficiency. One notable advancement in this direction was introduced by Aquilante *et al.*, who devised a two-step algorithm involving the determination of the Cholesky vectors followed by the construction of the 3-index ERI tensors.[19] Subsequently, Folkestad *et al.* optimized this approach by applying the density fitting formalism in the construction of the 3-index ERI tensors.[20] Recently, the two-step algorithm is further improved by the "dynamic-ERI" algorithm that tracks, saves, and reuses the important ERIs, discarding the non-essential ones.[21]

While the RI approach has demonstrated its effectiveness in nonrelativistic quantum chemistry calculations, its potential application in two-component and four-component relativistic electronic

theory has remained largely unexplored. The challenge arises from the need to effectively handle basis functions that exhibit diverse characteristics, including those associated with both large and small components.[25,26] In order to reduce the computational cost of relativistic electronic structure methods, RI with density fitting has been introduced.[27,28] However, the employment of RI in relativistic electronic structure methods raises concerns due to potential uncontrolled errors introduced by the density fitting approximation. Particularly, it is uncertain whether the application of RI can guarantee the fulfillment of physical and mathematical conditions, such as the variational stability, within the realm of relativistic methods.[25,26,29,30]

In this paper, we present a methodological advancement toward the development of an accurate and versatile RI technique for relativistic electronic structure theory. Specifically, we introduce the implementation of the Cholesky integral decomposition technique, which offers tunability and provides a systematic framework to assess the validity of RI in Dirac–Coulomb electronic structure methods, including numerical errors and their origins. Moreover, our objective is to investigate the extent to which the relativistic RI approach satisfies the variational stability in four-component methods. This research paves the way for utilizing approximate relativistic integrals within the context of Dirac–Coulomb electronic structure methods.

II. METHODOLOGY

A. Relativistic integrals for Dirac–Coulomb four-component calculations

The wave function of the Dirac equation in the four-spinor representation is

$$\Psi = \begin{pmatrix} \phi^L \\ \phi^S \end{pmatrix}, \tag{1}$$

where ϕ^L and ϕ^S denote spinors of the large (L) and small (S) component, respectively. The four-spinor molecular orbitals can also be expressed in a two-spinor basis as

$$\phi_p^L = \sum_\tau \sum_{\mu=1}^{N} c_{\mu\tau,p}^L \chi_{\mu\tau}^L, \tag{2}$$

$$\phi_p^S = \sum_\tau \sum_{\mu=1}^{N} c_{\mu\tau,p}^S \chi_{\mu\tau}^S,$$

$$\tau \in \{\alpha, \beta\}, \tag{3}$$

where N is the number of spatial orbitals. The large component spinor basis can be expressed as

$$\chi_{\mu\alpha}^L = \begin{pmatrix} \chi_\mu \\ 0 \end{pmatrix}, \quad \chi_{\mu\beta}^L = \begin{pmatrix} 0 \\ \chi_\mu \end{pmatrix}, \tag{4}$$

where χ_μ is the large-component spatial basis function. The small-component basis can be obtained from the large component basis via the restricted-kinetic-balance (RKB) condition, which ensures the correct nonrelativistic limit of the positive energy states,[25,26,29]

$$\chi_{\mu\tau}^S = \frac{1}{2mc} \boldsymbol{\sigma} \cdot \mathbf{p}\, \chi_{\mu\tau}^L. \tag{5}$$

Here, m represents mass of the electron, and c and $\mathbf{p}$ are the speed of light and linear momentum operator, respectively. $\boldsymbol{\sigma}$ is the vector of Pauli matrices.

The primary challenge in constructing the relativistic Dirac–Coulomb Hamiltonian lies in the computation of two-electron repulsion integrals within the atomic orbital (AO) basis. This involves calculating three distinct integral classes: a symmetric all large-component integral $(\mu^L \nu^L | \kappa^L \lambda^L)$, a symmetric all small-component integral $(\mu^S \nu^S | \kappa^S \lambda^S)$, and a mixed large- and small-component integral $(\mu^S \nu^S | \kappa^L \lambda^L)$, which does not have symmetry between electrons 1 and 2. The Mulliken notation is employed to denote these two-electron integrals. When applying the RKB condition [Eq. (5)] within the Dirac equation, the computation of $(\mu^S \nu^S | \kappa^L \lambda^L)$ and $(\mu^S \nu^S | \kappa^S \lambda^S)$ integrals requires the calculation of two-center and four-center integral derivatives. This process gives rise to integral forms, such as $(\nabla\mu \cdot \nabla\nu | \kappa\lambda)$ (scalar product) and $(\nabla\mu \times \nabla\nu | \kappa\lambda)$ (cross product), where the L or S notation on basis functions is no longer needed as they are all large-component basis functions.

Due to the fact that the basis set must also describe negative-energy states, it is important to use uncontracted basis sets in the SCF calculations so that this condition is fulfilled. The use of contracted large- and small-component functions from atomic Dirac-Hartree-Fock (DHF) calculations (atomic balance[31]) may lead to violation of the separation of the positive- and negative-energy states.[32]

Recent advancements utilizing the Pauli quaternion representation have achieved a minimum floating-point count algorithm for constructing the relativistic Hamiltonian in spin- and component-separated forms.[33–35] This approach allows for density-integral contraction directly using one-component scalar integrals. The Cholesky integral decomposition method introduced in this work is developed within the framework of relativistic Dirac–Coulomb Hamiltonian construction using the Pauli quaternion representation. In other words, scalar integrals are Cholesky-decomposed directly and employed in the Hamiltonian construction process.

B. Cholesky decomposition for relativistic Dirac–Coulomb integrals

A symmetric, positive semi-definite electron repulsion integral (ERI) matrix $\mathbf{M}$ can be approximated using the Cholesky decomposition technique as

$$M_{\mu\nu,\kappa\lambda} = (\mu\nu|\kappa\lambda) \approx \sum_{P \in \mathcal{B}} L_{\mu\nu}^P L_{\kappa\lambda}^P = (\mathbf{L}\mathbf{L}^\mathbf{T})_{\mu\nu,\kappa\lambda}, \tag{6}$$

where $L_{\mu\nu}^P$ is P-th component of the Cholesky vector matrix $\mathbf{L}$ and $\mathcal{B}$ contains all selected Cholesky pivots.

The Cholesky vectors are generated iteratively per index pair $(\mu\nu)$ using a pivoting procedure,[16] which starts with an empty $\mathcal{B}$ followed by setting the initial values of the residual diagonal elements as $\widetilde{(\mu\nu|\mu\nu)} = (\mu\nu|\mu\nu)$. At each iteration, a new Cholesky pivot $P \equiv \kappa\lambda$ corresponding to the largest residual diagonal element is selected, and the new Cholesky vector is described as

$$L_{\mu\nu}^P = \frac{(\mu\nu|P) - \sum_{R \in \mathcal{B}} L_{\mu\nu}^R L_P^R}{\widetilde{(P|P)}^{\frac{1}{2}}}, \tag{7}$$

where after every iteration, P is added to $\mathcal{B}$, and the residual diagonal elements are updated as

$$\widetilde{(\mu\nu|\mu\nu)} = \widetilde{(\mu\nu|\mu\nu)} - (L^P_{\mu\nu})^2. \tag{8}$$

This continues until the predefined Cholesky threshold τ becomes greater than the largest diagonal element.

In the two-step algorithm[20] to generate Cholesky vectors, the first-step involves determination of the Cholesky pivot set without computing the complete Cholesky vectors. This is followed by expressing Eq. (6) as an inner projection in a resolution-of-the-identity (RI) approach,

$$M_{\mu\nu,\kappa\lambda} \approx \sum_{P',P\in\mathcal{B}} (\mu\nu|P')(\mathbf{J}^{-1})_{P'P}(P|\kappa\lambda), \tag{9}$$

$$J_{PP'} = (P'|P), \qquad P,P' \in \mathcal{B}. \tag{10}$$

The Cholesky vectors can be formed by Cholesky decomposing $\mathbf{J} = \mathbf{Q}\mathbf{Q}^{\mathrm{T}}$,

$$L^P_{\mu\nu} = \sum_{P'\in\mathcal{B}} (\mu\nu|P')(\mathbf{Q}^{-\mathrm{T}})_{P'P}, \tag{11}$$

where $\mathbf{Q}$ is a lower triangular matrix and $\mathbf{Q}^{-\mathrm{T}} \equiv (\mathbf{Q}^{\mathrm{T}})^{-1}$.

As mentioned in Sec. II A, the construction of the Dirac–Coulomb Hamiltonian involves the computation of three integral types: $(\mu\nu|\kappa\lambda)$ or $(LL|LL)$, $(\nabla\mu\nabla\nu|\kappa\lambda)$ or $(SS|LL)$, and $(\nabla\mu\nabla\nu|\nabla\kappa\nabla\lambda)$ or $(SS|SS)$. It is straightforward to apply the Cholesky decomposition method to the symmetric large-component-only integrals $(LL|LL)$ as this is equivalent to its application in nonrelativistic theory. Determining the appropriate strategy for obtaining Cholesky vectors for the $(SS|LL)$ integrals is not as clear-cut as this matrix is not symmetric. Decomposing the $(SS|SS)$ integrals, which are also symmetric, is considerably more work than decomposing the $(LL|LL)$ integrals due to the need to compute fourth-order integral derivatives.

A simple strategy is to use the Cholesky pivots obtained for the symmetric large-component-only integrals $(LL|LL)$ to compute Cholesky vectors for all unique terms in small-component integrals,

$$L^P_{\tilde{\mu}\tilde{\nu}} = \sum_{P'\in\mathcal{B}} (\tilde{\mu}\tilde{\nu}|P')(\mathbf{Q}^{-T})_{P'P}, \tag{12}$$

$$(\tilde{\mu}\tilde{\nu}|\kappa\lambda) = \sum_{P\in\mathcal{B}} L^P_{\tilde{\mu}\tilde{\nu}} L^P_{\kappa\lambda}, \tag{13}$$

$$(\tilde{\mu}\tilde{\nu}|\bar{\kappa}\bar{\lambda}) = \sum_{P\in\mathcal{B}} L^P_{\tilde{\mu}\tilde{\nu}} L^P_{\bar{\kappa}\bar{\lambda}}, \tag{14}$$

where $\tilde{\mu} \equiv \nabla\mu$. It is important to note that the same small-component Cholesky vectors $L^P_{\tilde{\mu}\tilde{\nu}}$ are used for calculating the $(SS|SS)$ integrals without any additional computational cost as required in the exact formalism. In the subsequent discussion, we will refer to this technique as the Restricted-Kinetic-Balance Resolution-of-the-Identity (RKB-RI) approach with Cholesky integral decomposition.

This simple strategy relies on the fact that the large-component atomic basis for the most part adequately covers the small-component atomic basis: the s functions are a good representation of the basis for the small component of the $p_{1/2}$ spinors, the p functions are a good representation of the basis for the small component of the $s_{1/2}$ spinors, and so on. The only functions present in the small-component basis that are not present in the large-component basis are the functions of the highest angular momentum. However, as the Cholesky vectors represent the density and not directly the basis functions themselves, most of the density described by these high angular momentum functions is covered by the Cholesky vectors. For the part that is not covered, the small component is sufficiently small that the error is also small.

C. Error analysis for relativistic Cholesky integral decomposition

A unique advantage of Cholesky integral decomposition is that it builds the auxiliary basis on-the-fly to any order of accuracy for any basis set and any chemical system. In other words, the Cholesky decomposition approach is versatile and the accuracy is tunable via a user-defined threshold τ.

Using $\widetilde{\mathbf{M}}$ to represent the difference between the exact matrix $\mathbf{M}$ and approximate $L^P_{\mu\nu}L^P_{\kappa\lambda}$, the error in Cholesky decomposition for the large-component $(LL|LL)$ integrals can be computed according to the Cauchy–Schwarz inequality,[16]

$$\left(\widetilde{M}_{\mu\nu,\kappa\lambda}\right)^2 \le \widetilde{M}_{\mu\nu,\mu\nu} \cdot \widetilde{M}_{\kappa\lambda,\kappa\lambda} \le \tau^2. \tag{15}$$

Thus, τ provides an upper-bound to the maximum error of the Cholesky decomposition approximation for the $(LL|LL)$ integral.

However, the same analysis cannot be applied to determine the error in the $(SS|LL)$ integrals due to their asymmetric nature. To estimate the accuracy of the Cholesky decomposition approximation for $(SS|LL)$ integrals, we describe the difference in the exact and the residual ERI matrix as

$$\widetilde{M}_{\tilde{\mu}\tilde{\nu},\kappa\lambda} = M_{\tilde{\mu}\tilde{\nu},\kappa\lambda} - \sum_{P\in\mathcal{B}} L^P_{\tilde{\mu}\tilde{\nu}} L^P_{\kappa\lambda}, \tag{16}$$

followed by application of the Cauchy–Schwarz inequality

$$\left(\widetilde{M}_{\tilde{\mu}\,\tilde{\nu},\kappa\lambda}\right)^2 \le \widetilde{M}_{\tilde{\mu}\tilde{\nu},\tilde{\mu}\tilde{\nu}} \cdot \widetilde{M}_{\kappa\lambda,\kappa\lambda} \le \widetilde{M}_{\tilde{\mu}\tilde{\nu},\tilde{\mu}\tilde{\nu}} \cdot \tau \le \max\left(|\widetilde{M}_{\tilde{\mu}\tilde{\nu},\tilde{\mu}\tilde{\nu}}|\right) \cdot \tau$$
$$\widetilde{M}_{\tilde{\mu}\tilde{\nu},\tilde{\mu}\tilde{\nu}} = M_{\tilde{\mu}\tilde{\nu},\tilde{\mu}\tilde{\nu}} - \sum_{P\in\mathcal{B}} L^P_{\tilde{\mu}\tilde{\nu}} L^P_{\bar{\kappa}\bar{\lambda}}. \tag{17}$$

Equation (17) suggests that the error in the $(SS|LL)$ integrals is not bounded by the large-component Cholesky threshold τ. The same applies for the $(SS|SS)$ integrals. It is important to note that since these errors are not bounded, there is a possibility of variational collapse during four-component calculations. To assess the suitability and reliability of the RKB-RI approach in four-component Dirac–Coulomb calculations, Sec. III will utilize numerical benchmarks for validation.

III. RESULTS AND DISCUSSION

All calculations are performed with a development version of the Chronus Quantum software package.[36] The speed of light utilized is 137.035 999 074 a.u. The uncontracted ANO-RCC-VDZP[37] basis set was utilized, resulting in 239 basis functions with up to f orbital angular momentum for Au atom. Convergence thresholds of 10^{-9} a.u. in energy and 10^{-7} a.u in densities and gradients were used.

A. Accuracy of RKB-RI with Cholesky decomposition

When employing the RKB-RI approximation to estimate relativistic two-electron integrals, it is possible that the SS density is not adequately described by the large-component Cholesky vectors. Thus, there is an extra source of error over the error in the large-component integral decomposition, as discussed in Sec. II B. Here, we investigate this issue to ensure that calculations with the RKB-RI approximations provide accurate and reliable results.

Table I shows the total four-component Hartree–Fock energy computed using the Dirac–Coulomb Hamiltonian with the RI formalism for an isolated Au atom with an uncontracted ANO-RCC-VDZP basis at different Cholesky thresholds. Increasing the threshold leads to an increased error in the ground state energies of the Au atom compared to the energy computed using full electron repulsion integrals (ERIs). The RKB-RI approach produces energies slightly lower than those obtained using full 4-index integrals for some values of τ. However, this behavior is commonly observed in RI approaches within nonrelativistic theory, and the RKB-RI approach remains highly reliable and robust, making it an excellent choice for accurate energy calculations.

In contrast to nonrelativistic calculations, where only a single type of ERI $(LL|LL)$ is typically considered, the use of the Dirac–Coulomb Hamiltonian involves additional ERIs, namely, $(SS|LL)$ and $(SS|SS)$. These ERIs have a prefactor of $\frac{1}{(2mc)^2}$ and $\frac{1}{(2mc)^4}$, respectively, in the energy expression, where m represents the mass of the electron and c denotes the speed of light. The construction of these ERIs from several scalar integrals adheres to the principles of the RKB condition.

Table II shows the mean integral values and mean absolute errors of different scalar integrals at a Cholesky-decomposition threshold of $\tau = 10^{-5}$. Integrals involving scalar products of the small-component bases, including $(\nabla_\mu \cdot \nabla_\nu)(\mu\nu|\kappa\lambda)$ and $(\nabla_\mu \cdot \nabla_\nu)(\nabla_\kappa \cdot \nabla_\lambda)(\mu\nu|\kappa\lambda)$, representing direct Coulombic interactions for large-small and small-small components of the wave function, produce larger mean absolute errors than the $(LL|LL)$ integral. This is understandable as the auxiliary Cholesky-decomposition bases are constructed using the large-component basis that cannot form the complete set to map small-component bases to the auxiliary bases. The error is the largest for the full scalar product of the $(SS|SS)$ term. Nevertheless, they fall below the predicted errors calculated according to Eq. (17), as shown in Table S1 in the supplementary material.

TABLE I. Errors in the ground state energies of an Au atom computed using the Cholesky-decomposed four-component Dirac–Coulomb Hartree–Fock theory with an uncontracted ANO-RCC-VDZP basis (total 239 basis functions) at different Cholesky-decomposition thresholds, relative to exact integrals.[a,b]

τ	Auxiliary basis	RI energy (E_h)	RI errors (E_h)
10^{-9}	1908	−19 035.579 061 628 8	1.3×10^{-8}
10^{-8}	1727	−19 035.579 061 661 0	-1.9×10^{-8}
10^{-7}	1593	−19 035.579 061 839 1	-2.0×10^{-7}
10^{-6}	1474	−19 035.579 055 212 6	6.4×10^{-6}
10^{-5}	1298	−19 035.578 985 937 5	7.6×10^{-5}
10^{-4}	1090	−19 035.578 036 725 7	1.2×10^{-3}
10^{-3}	881	−19 035.574 049 534 3	5.0×10^{-3}
10^{-2}	635	−19 035.325 003 680 7	2.5×10^{-1}
10^{-1}	322	−19 027.295 741 948 7	$8.3 \times 10^{+0}$

[a]Dirac–Coulomb Hartree–Fock energy using exact integrals: −19 035.579 061 641 9 E_h.
[b]Numerical grid (Ref. 38) −19 035.595 10 E_h.

TABLE II. Mean integral value (MIV) and mean absolute errors (MAE) of all Dirac–Coulomb scalar integrals computed at Cholesky-decomposition threshold of $\tau = 10^{-4}$ for Au_2 with a fully uncontracted ANO-RCC basis (594 basis functions). Integrals involving small-component, $(SS|LL)$ and $(SS|SS)$, have been scaled with prefactors of $\frac{1}{(2mc)^2}$ and $\frac{1}{(2mc)^4}$, respectively. The four-component Dirac–Coulomb Hartree–Fock energies are as follows: $E_{\text{exact}} = -38\,071.189\,901\ E_h$ and $\Delta E_{\text{RI}} = 1.3 \times 10^{-3}\ E_h$.

Block	ERI component	MIV	MAE
$(LL\|LL)$:			
	$(\mu\nu\|\kappa\lambda)$	1.7×10^{-4}	1.7×10^{-9}
$(SS\|LL)$:			
	$(\nabla_\mu \cdot \nabla_\nu)(\mu\nu\|\kappa\lambda)$	1.6×10^{-2}	4.1×10^{-9}
	$(\nabla_\mu \times \nabla_\nu)_x(\mu\nu\|\kappa\lambda)$	1.3×10^{-3}	7.9×10^{-11}
	$(\nabla_\mu \times \nabla_\nu)_y(\mu\nu\|\kappa\lambda)$	1.3×10^{-3}	7.9×10^{-11}
	$(\nabla_\mu \times \nabla_\nu)_z(\mu\nu\|\kappa\lambda)$	1.3×10^{-3}	6.7×10^{-11}
$(SS\|SS)$:			
	$(\nabla_\mu \cdot \nabla_\nu)(\nabla_\kappa \cdot \nabla_\lambda)(\mu\nu\|\kappa\lambda)$	4.9×10^{0}	9.2×10^{-5}
	$(\nabla_\mu \times \nabla_\nu)_x(\nabla_\kappa \cdot \nabla_\lambda)(\mu\nu\|\kappa\lambda)$	4.1×10^{-1}	8.6×10^{-7}
	$(\nabla_\mu \times \nabla_\nu)_y(\nabla_\kappa \cdot \nabla_\lambda)(\mu\nu\|\kappa\lambda)$	4.1×10^{-1}	8.6×10^{-7}
	$(\nabla_\mu \times \nabla_\nu)_z(\nabla_\kappa \cdot \nabla_\lambda)(\mu\nu\|\kappa\lambda)$	4.1×10^{-1}	7.3×10^{-7}
	$(\nabla_\mu \times \nabla_\nu)_x(\nabla_\kappa \times \nabla_\lambda)_x(\mu\nu\|\kappa\lambda)$	3.0×10^{-1}	2.5×10^{-8}
	$(\nabla_\mu \times \nabla_\nu)_x(\nabla_\kappa \times \nabla_\lambda)_y(\mu\nu\|\kappa\lambda)$	1.7×10^{-1}	2.4×10^{-8}
	$(\nabla_\mu \times \nabla_\nu)_x(\nabla_\kappa \times \nabla_\lambda)_z(\mu\nu\|\kappa\lambda)$	1.7×10^{-1}	2.0×10^{-8}
	$(\nabla_\mu \times \nabla_\nu)_y(\nabla_\kappa \times \nabla_\lambda)_y(\mu\nu\|\kappa\lambda)$	3.0×10^{-1}	2.5×10^{-8}
	$(\nabla_\mu \times \nabla_\nu)_y(\nabla_\kappa \times \nabla_\lambda)_z(\mu\nu\|\kappa\lambda)$	1.7×10^{-1}	2.0×10^{-8}
	$(\nabla_\mu \times \nabla_\nu)_z(\nabla_\kappa \times \nabla_\lambda)_z(\mu\nu\|\kappa\lambda)$	3.0×10^{-1}	1.7×10^{-8}

B. Computational cost analysis

The main advantage of using RKB-RI integrals is that it avoids recomputation of 4-index ERIs by storing 3-index Cholesky vectors and forming the Hamiltonian matrix directly in memory, i.e., in-core algorithm. Table III shows the relative timings along with the individual cost for Coulomb (**J**) and exchange (**K**) contractions in each SCF iteration using different in-core algorithms for Ag_2 simulated using a moderate-sized basis.

When comparing the two algorithms, it is evident that the 4-index in-core Fock-build is faster than the RKB-RI formalism. Taking a closer look at the in-core timings, we observe that the computation of RKB-RI Coulomb **J** terms is significantly faster than the corresponding 4-index Coulomb build. This is primarily due to the reduction in scaling, transitioning from N_{basis}^4 when using 4-index integrals to $N_{\text{basis}}^2 N_{\text{aux}}$ with the RKB-RI formalism for the Coulomb **J** build. However, it is important to note that the exchange **K** contraction with RKB-RI integrals scales as $N_{\text{basis}}^3 N_{\text{aux}}$, which can be computationally more demanding compared to the N_{basis}^4 scaling of the 4-index in-core formalism when $N_{\text{aux}} > N_{\text{basis}}$.

Upon analyzing the computational costs associated with each Fock matrix block, it becomes evident that the all small-component

TABLE III. Cost[a] comparison of in-core 4-index and in-core RKB-RI algorithms using ANO-RCC-VDZP basis (364 basis functions[b]).

	4-Index in-core			RKB-RI in-core		
Fock matrix block	Total	**J**	**K**	Total	**J**	**K**
$\mathbf{F}^{LL}$	1.00	0.33	0.67	1.69	0.01	1.68
$\mathbf{F}^{\mathrm{SL}}$	0.71	⋯	0.71[c]	6.56	⋯	6.56[c]
$\mathbf{F}^{SS}$	14.54	3.83	10.71	26.96	0.05	26.91

[a]Cost is measured relative to the large-component block $\mathbf{F}^{LL}$ calculation with 4-index integrals.
[b]The Cholesky-decomposition threshold is 10^{-4}, resulting in 1558 auxiliary bases.
[c]The SL block of the Fock matrix has exchange contribution only.

block $\mathbf{F}^{SS}$ incurs significantly higher expenses compared to other blocks. This increased cost primarily arises from the additional contractions involving the $(SS|SS)$ integrals, as illustrated in Table II. Enhancing the computational efficiency by employing RKB-RI for the small-large component block of the Fock matrix $\mathbf{F}^{\mathrm{SL}}$ proves to be more challenging, given its exclusive reliance on exchange interactions.

These observations highlight the trade-offs in performance between the different algorithms employed. The choice between 4-index and RKB-RI in-core approaches depends on the specific computational requirements, memory size, and the nature of the Hamiltonian (e.g., **J** vs **K**).

C. Benchmark: Properties of actinyl oxides

In this section, we benchmark the performance of the RKB-RI algorithm using Cholesky vectors for three actinyl oxides: UO_2^{2+}, NpO_2^{2+}, and PuO_2^{2+}. In addition to the absolute ground state energies, we also focus on other properties, such as the potential energy surfaces (PESs), equilibrium bond lengths, and atomization energies. We use the four-component Dirac–Coulomb Hartree–Fock calculations as our reference for comparison. All calculations were performed with linear geometries with experimental bond lengths of 1.76, 1.75, and 1.74 Å for U–O, Np–O, and Pu–O, respectively.[39] An uncontracted ANO-RCC-VDZP basis and a Cholesky-decomposition threshold of $\tau = 10^{-4}$ were used for all present calculations. Computational results presented herein are not compared to experiments because these benchmark studies are intended for the sole purpose of determining the accuracy of RKB-RI relative to the exact method.

1. Ground state energies

Table IV presents the errors in the ground state energies computed with the approximate RKB-RI integrals. As expected, the errors decrease with tighter threshold consistently for all the actinyls. The different signs of the errors signify that the RKB-RI technique for Dirac–Coulomb Hartree–Fock is not variational or bound from below by the exact result using 4-index integrals. The major contribution to the overall error stems from the $(LL|LL)$ component, whereas the smaller errors of the $(SS|LL)$ to $(SS|SS)$ can be explained due to their contributions of the order of $\frac{1}{c^2}$ and $\frac{1}{c^4}$, respectively, to the total Dirac-Coulomb energy. A fraction of the errors in the small-component energies also comes from the projection of the large-component Cholesky vectors on to the small-component one. Fortunately, we do not observe a variational collapse at higher thresholds, which validates the success of the RKB condition in this Cholesky decomposed relativistic formalism.

2. Potential energy surface

In Fig. 1, we present the potential energy surface (PES) plots obtained using both the exact 4-index integrals and the RKB-RI integrals. It is worth noting that, overall, the two methods yield qualitatively similar PES plots for all the oxides. However, there are quantitative differences that can be observed, with discrepancies of ~0.002 to 0.003 a.u. Among the oxides, the largest deviation is observed for PuO_2^{2+}, particularly around the equilibrium point. The differences in energy calculations for this system are more pronounced compared to the other oxides.

To provide further insight, Table V presents the equilibrium bond lengths obtained from the PES scans for the three actinyl oxides. Notably, the RKB-RI method exhibits the highest error for

TABLE IV. Analysis of the errors in the ground state energies of a series of actinyl oxides, UO_2^{2+}, NpO_2^{2+}, and PuO_2^{2+}, computed using the four-component Dirac–Coulomb Hartree–Fock theory with an uncontracted ANO-RCC-VDZP basis (438 basis functions) and Cholesky-decomposed RKB-RI integrals.

				Component-wise RKB-RI errors (E_h)		
System	τ	Auxiliary basis no.	Errors (E_h)	$(LL\|LL)$	$(SS\|LL)$	$(SS\|SS)$
UO_2^{2+}	10^{-4}	1858	2.1×10^{-3}	1.9×10^{-3}	2.0×10^{-4}	3.6×10^{-6}
	10^{-5}	2363	1.3×10^{-4}	1.4×10^{-4}	-6.6×10^{-6}	6.1×10^{-8}
	10^{-9}	4078	9.5×10^{-9}	9.1×10^{-9}	6.0×10^{-10}	-2.0×10^{-10}
NpO_2^{2+}	10^{-4}	1864	1.9×10^{-3}	1.8×10^{-3}	1.9×10^{-4}	3.3×10^{-6}
	10^{-5}	2361	1.4×10^{-4}	1.4×10^{-4}	-2.1×10^{-7}	9.0×10^{-8}
	10^{-9}	4082	-5.2×10^{-9}	-4.4×10^{-9}	-5.0×10^{-10}	-3.0×10^{-10}
PuO_2^{2+}	10^{-4}	1862	2.0×10^{-3}	1.9×10^{-3}	1.6×10^{-4}	2.8×10^{-6}
	10^{-5}	2370	1.4×10^{-4}	1.4×10^{-4}	-1.9×10^{-7}	6.9×10^{-8}
	10^{-9}	4081	5.2×10^{-9}	5.7×10^{-9}	-3.0×10^{-10}	-2.0×10^{-10}

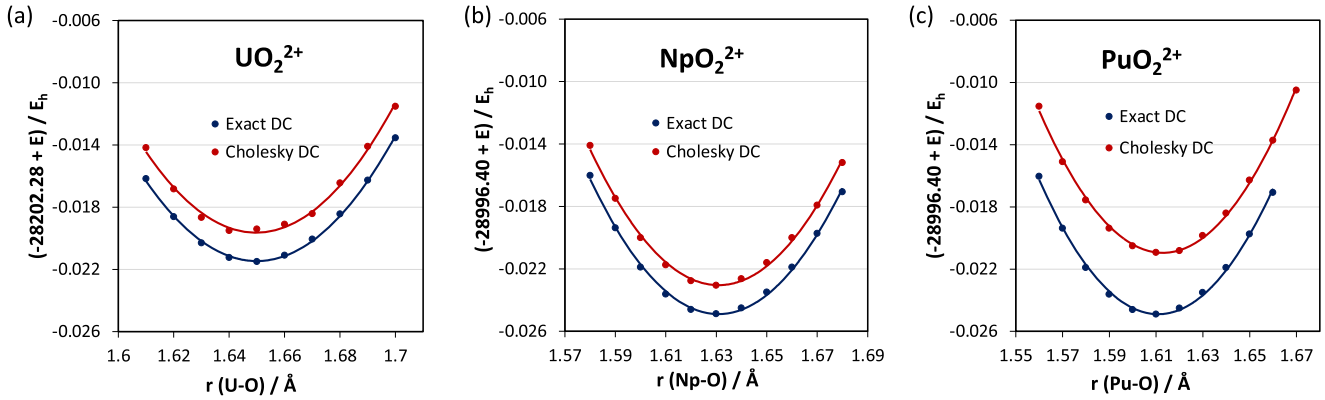

FIG. 1. Potential energy surface plots for a series of actinyl oxides, UO_2^{2+}, NpO_2^{2+}, and PuO_2^{2+}, computed using the four-component Dirac–Coulomb Hartree–Fock theory with an uncontracted ANO-RCC-VDZP basis and Cholesky-decomposed RKB-RI integrals.

TABLE V. Equilibrium bond lengths for a series of actinyl oxides, UO_2^{2+}, NpO_2^{2+}, and PuO_2^{2+}, computed using the four-component Dirac–Coulomb Hartree–Fock theory with an uncontracted ANO-RCC-VDZP basis and Cholesky-decomposed RKB-RI integrals.

System	Exact (Å)	RKB-RI (Å)	Errors (Å)
UO_2^{2+}	1.6450	1.6497	4.70×10^{-3}
NpO_2^{2+}	1.6319	1.6318	-1.00×10^{-4}
PuO_2^{2+}	1.6132	1.6129	-3.00×10^{-4}

UO_2^{2+}, with a discrepancy of ~0.005 Å. On the other hand, the errors for the remaining two oxides are of the order of $\sim 10^{-4}$ Å, indicating a comparatively lower level of deviation. Despite variations in the PES plots, the essential characteristic of the bond lengths remains consistent.

Our next set of tests involved computing the atomization energies of the actinyl oxides into $2 \times O^{2-}$ and the respective An(VI) ions, as shown in Table VI. The atomization energies increase with increasing atomic number of the actinide atom, although the RKB-RI errors do not seem to follow any particular trend. Overall, RKB-RI errors in the atomization energies are of the order $\sim 10^{-4}$ eV, with UO_2^{2+} producing the highest error (~0.005 eV), but still well below the chemical accuracy.

TABLE VI. Ground state bond atomization energies of three actinyl oxides computed as $\Delta E = 2 \times E(O^{2-}) + E(\mathrm{An(VI)}) - E(AnO_2^{2+})$, computed using the four-component Dirac–Coulomb Hartree–Fock theory with an uncontracted ANO-RCC-VDZP basis and Cholesky-decomposed RKB-RI integrals.

System	Exact (eV)	RKB-RI (eV)	Error (eV)
UO_2^{2+}	178.907 654 9	178.902 670 2	-4.98×10^{-3}
NpO_2^{2+}	182.636 063 3	182.635 211 2	-8.52×10^{-4}
PuO_2^{2+}	186.544 183 9	186.548 446 7	4.26×10^{-3}

IV. CONCLUSIONS AND PERSPECTIVE

In this work, we introduce the implementation of the two-step Cholesky decomposition technique to aid in the in-core relativistic four-component Hamiltonian-build using resolution-of-the-identity within the restricted-kinetic-balance condition (RKB-RI). We presented a recipe that uses large-component Cholesky pivots for computing RKB-RI integrals involving small-component bases and associated error-analysis techniques for different Dirac–Coulomb integral components.

In order to thoroughly evaluate the capabilities and accuracy of the Cholesky-decomposed RKB-RI algorithm, we conducted benchmark calculations to assess its performance in various aspects, including ground state energies, potential energy scans, equilibrium bond lengths, and atomization energies for a series of actinyl oxides. The results indicate that while there may be discernible differences in computed energy values between the 4-index and RKB-RI algorithms, the calculated chemical properties, particularly the equilibrium bond lengths and atomization energies, exhibit a high degree of agreement between the two methods. The absence of variational collapse or prolapse in the computed energies is a significant aspect that affirms the stability of the RKB-RI approach in four-component calculations.

The cost analysis conducted demonstrates that the Cholesky-decomposed RKB-RI algorithm offers several advantages. First, it reduces the storage requirements for integrals, thereby optimizing memory usage. Additionally, it significantly decreases the computational cost associated with Coulomb contraction, compared to utilizing 4-index integrals. However, it is important to note that the exchange part of the Hamiltonian build using RKB-RI can be more computationally demanding when the number of Cholesky vectors surpasses the number of large-component basis functions.

SUPPLEMENTARY MATERIAL

The supplementary material includes predicted and observed maximum errors for Au_2.

ACKNOWLEDGMENTS

S.B. acknowledges support from the Center for MAny-Body Methods, Spectroscopies, and Dynamics for Molecular POLaritonic Systems (MAPOL) under subcontract from FWP79715, which is funded as part of the Computational Chemical Sciences (CCS) program by the U.S. Department of Energy, Office of Science, Office of Basic Energy Sciences, Division of Chemical Sciences, Geosciences and Biosciences at the Pacific Northwest National Laboratory (PNNL). PNNL is a multi-program national laboratory operated by Battelle Memorial Institute for the United States Department of Energy under DOE Contract No. DE-AC05-76RL1830. The development of the Chronus Quantum computational software is supported by the Office of Advanced Cyberinfrastructure, National Science Foundation (Grant No. OAC-2103717 to X.L.). Computations were facilitated through the use of advanced computational, storage, and networking infrastructure provided by the shared facility supported by the University of Washington Molecular Engineering Materials Center (Grant No. DMR-1719797) via the Hyak supercomputer system.

AUTHOR DECLARATIONS

Conflict of Interest

The authors have no conflicts to disclose.

Author Contributions

S. Banerjee and T. Y. Zhang are co-first authors. These authors contributed equally to this work.

Samragni Banerjee: Data curation (lead); Formal analysis (lead); Investigation (lead); Methodology (equal); Software (equal); Validation (lead); Writing – original draft (lead); Writing – review & editing (equal). **Tianyuan Zhang**: Conceptualization (equal); Formal analysis (equal); Investigation (equal); Methodology (equal); Project administration (equal); Software (lead); Supervision (equal); Validation (equal); Writing – original draft (supporting); Writing – review & editing (supporting). **Kenneth G. Dyall**: Conceptualization (equal); Methodology (equal); Writing – review & editing (supporting). **Xiaosong Li**: Conceptualization (lead); Data curation (supporting); Formal analysis (equal); Funding acquisition (lead); Investigation (equal); Methodology (equal); Project administration (lead); Resources (lead); Software (equal); Supervision (equal); Validation (equal); Visualization (equal); Writing – original draft (equal); Writing – review & editing (lead).

DATA AVAILABILITY

The data that support the findings of this study are available within the article and its supplementary material. Additional data can be made available from the corresponding author upon reasonable request.

REFERENCES

[1] L. Freitag, S. Knecht, C. Angeli, and M. Reiher, "Multireference perturbation theory with Cholesky decomposition for the density matrix renormalization group," J. Chem. Theory Comput. **13**, 451 (2017).

[2] M. Lesiuk, "Implementation of the coupled-cluster method with single, double, and triple excitations using tensor decompositions," J. Chem. Theory Comput. **16**, 453–467 (2020).

[3] U. Bozkaya, "Efficient implementation of the second-order quasidegenerate perturbation theory with density-fitting and Cholesky decomposition approximations: Is it possible to use Hartree–Fock orbitals for a multiconfigurational perturbation theory?," J. Chem. Theory Comput. **15**, 4415–4429 (2019).

[4] K. P. Hannon, C. Li, and F. A. Evangelista, "An integral-factorized implementation of the driven similarity renormalization group second-order multireference perturbation theory," J. Chem. Phys. **144**, 204111 (2016).

[5] T. Zhang, C. Li, and F. A. Evangelista, "Improving the efficiency of the multireference driven similarity renormalization group via sequential transformation, density fitting, and the noninteracting virtual orbital approximation," J. Chem. Theory Comput. **15**, 4399–4414 (2019).

[6] M. Motta, J. Shee, S. Zhang, and G. K.-L. Chan, "Efficient ab initio auxiliary-field quantum Monte Carlo calculations in Gaussian bases via low-rank tensor decomposition," J. Chem. Theory Comput. **15**, 3510–3521 (2019).

[7] J. Fosso-Tande, T.-S. Nguyen, G. Gidofalvi, and A. E. DePrince III, "Large-scale variational two-electron reduced-density-matrix-driven complete active space self-consistent field methods," J. Chem. Theory Comput. **12**, 2260–2271 (2016).

[8] E. Epifanovsky, D. Zuev, X. Feng, K. Khistyaev, Y. Shao, and A. I. Krylov, "General implementation of the resolution-of-the-identity and Cholesky representations of electron repulsion integrals within coupled-cluster and equation-of-motion methods: Theory and benchmarks," J. Chem. Phys. **139**, 134105 (2013).

[9] C. D. Sherrill, "Frontiers in electronic structure theory," J. Chem. Phys. **132**, 110902 (2010).

[10] E. G. Hohenstein and C. D. Sherrill, "Density fitting and Cholesky decomposition approximations in symmetry-adapted perturbation theory: Implementation and application to probe the nature of π-π interactions in linear acenes," J. Chem. Phys. **132**, 184111 (2010).

[11] F. Aquilante, T. B. Pedersen, R. Lindh, B. O. Roos, A. Sánchez de Merás, and H. Koch, "Accurate *ab initio* density fitting for multiconfigurational self-consistent field methods," J. Chem. Phys. **129**, 024113 (2008).

[12] N. H. Beebe and J. Linderberg, "Simplifications in the generation and transformation of two-electron integrals in molecular calculations," Int. J. Quantum Chem. **12**, 683–705 (1977).

[13] I. Røeggen and E. Wisløff-Nilssen, "On the Beebe-Linderberg two-electron integral approximation," Chem. Phys. Lett. **132**, 154–160 (1986).

[14] F. Aquilante, R. Lindh, and T. B. Pedersen, "Unbiased auxiliary basis sets for accurate two-electron integral approximations," J. Chem. Phys. **127**, 114107 (2007).

[15] F. Aquilante, L. Gagliardi, T. B. Pedersen, and R. Lindh, "Atomic Cholesky decompositions: A route to unbiased auxiliary basis sets for density fitting approximation with tunable accuracy and efficiency," J. Chem. Phys. **130**, 154107 (2009).

[16] H. Koch, A. Sánchez de Merás, and T. B. Pedersen, "Reduced scaling in electronic structure calculations using Cholesky decompositions," J. Chem. Phys. **118**, 9481–9484 (2003).

[17] L. Boman, H. Koch, and A. Sánchez de Merás, "Method specific Cholesky decomposition: Coulomb and exchange energies," J. Chem. Phys. **129**, 134107 (2008).

[18] I. Røeggen and T. Johansen, "Cholesky decomposition of the two-electron integral matrix in electronic structure calculations," J. Chem. Phys. **128**, 194107 (2008).

[19] F. Aquilante, L. Boman, J. Boström, H. Koch, R. Lindh, A. S. de Merás, and T. B. Pedersen, in *Linear-Scaling Techniques in Computational Chemistry and Physics: Methods and Applications*, edited by R. Zalesny, M. G. Papadopoulos, P. G. Mezey, and J. Leszczynski (Springer Netherlands, Dordrecht, 2011), pp. 301–343.

[20] S. D. Folkestad, E. F. Kjønstad, and H. Koch, "An efficient algorithm for Cholesky decomposition of electron repulsion integrals," J. Chem. Phys. **150**, 194112 (2019).

[21] T. Zhang, X. Liu, E. F. Valeev, and X. Li, "Toward the minimal floating operation count Cholesky decomposition of electron repulsion integrals," J. Phys. Chem. A **125**, 4258–4265 (2021).
[22] B. I. Dunlap, J. W. D. Connolly, and J. R. Sabin, "On some approximations in applications of $X\alpha$ theory," J. Chem. Phys. **71**, 3396–3402 (1979).
[23] R. A. Kendall and H. A. Früchtl, "The impact of the resolution of the identity approximate integral method on modern ab initio algorithm development," Theor. Chem. Acc. **97**, 158–163 (1997).
[24] J. L. Whitten, "Coulombic potential energy integrals and approximations," J. Chem. Phys. **58**, 4496–4501 (1973).
[25] K. G. Dyall and K. Fægri, Jr., *Introduction to Relativistic Quantum Chemistry* (Oxford University Press, 2007).
[26] M. Reiher and A. Wolf, *Relativistic Quantum Chemistry: The Fundamental Theory of Molecular Science* (John Wiley & Sons, 2014).
[27] M. S. Kelley and T. Shiozaki, "Large-scale Dirac-Fock-Breit method using density fitting and 2-spinor basis functions," J. Chem. Phys. **138**, 204113 (2013).
[28] M. Repisky, S. Komorovsky, M. Kadek, L. Konecny, U. Ekström, E. Malkin, M. Kaupp, K. Ruud, O. L. Malkina, and V. G. Malkin, "ReSpect: Relativistic spectroscopy DFT program package," J. Chem. Phys. **152**, 184101 (2020).
[29] W. Liu, "Ideas of relativistic quantum chemistry," Mol. Phys. **108**, 1679–1706 (2010).
[30] S. Sun, T. F. Stetina, T. Zhang, and X. Li, "Chapter 10—On the finite nuclear effect and Gaussian basis set for four-component Dirac Hartree-Fock calculations," in *Rare Earth Elements and Actinides: Progress in Computational Science Applications*, edited by D. A. Penchoff, T. L. Windus, and C. C. Peterson (American Chemical Society, 2021), Vol. 1388, pp. 207–218.
[31] L. Visscher, P. J. C. Aerts, O. Visser, and W. C. Nieuwpoort, "Kinetic balance in contracted basis sets for relativistic calculations," Int. J. Quantum Chem. **40**, 131–139 (1991).
[32] K. G. Dyall, "Relativistic double-zeta, triple-zeta, and quadruple-zeta basis sets for the 7p elements, with atomic and molecular applications," Theor. Chem. Acc. **131**, 1172 (2012).
[33] S. Sun, T. F. Stetina, T. Zhang, H. Hu, E. F. Valeev, Q. Sun, and X. Li, "Efficient four-component Dirac–Coulomb–Gaunt Hartree–Fock in the Pauli spinor representation," J. Chem. Theory Comput. **17**, 3388–3402 (2021).
[34] S. Sun, J. N. Ehrman, Q. Sun, and X. Li, "Efficient evaluation of the Breit operator in the Pauli spinor basis," J. Chem. Phys. **157**, 064112 (2022).
[35] S. Sun, J. Ehrman, T. Zhang, Q. Sun, K. G. Dyall, and X. Li, "Scalar Breit interaction for molecular calculations," J. Chem. Phys. **158**, 171101 (2023).
[36] D. B. Williams-Young, A. Petrone, S. Sun, T. F. Stetina, P. Lestrange, C. E. Hoyer, D. R. Nascimento, L. Koulias, A. Wildman, J. Kasper, J. J. Goings, F. Ding, A. E. DePrince III, E. F. Valeev, and X. Li, "The Chronus Quantum software package," Wiley Interdiscip. Rev.: Comput. Mol. Sci. **10**, e1436 (2020).
[37] B. O. Roos, R. Lindh, P. Å. Malmqvist, V. Veryazov, and P. O. Widmark, "New relativistic ANO basis sets for transition metal atoms," J. Phys. Chem. A **109**, 6575–6579 (2005).
[38] L. Visscher and K. G. Dyall, "Dirac-Fock atomic electronic structure calculations using different nuclear charge distributions," At. Data Nucl. Data Tables **67**, 207–224 (1997).
[39] D.-C. Sergentu, T. J. Duignan, and J. Autschbach, "Ab initio study of covalency in the ground versus core-excited states and X-ray absorption spectra of actinide complexes," J. Phys. Chem. Lett. **9**, 5583–5591 (2018).